Chemical Engineering Journal 505 (2025) 158356

Contents lists available at ScienceDirect

Chemical Engineering Journal

journal homepage: www.elsevier.com/locate/cej

Simultaneous photocatalytic CO_2 reduction and C-C coupling of benzyl alcohol under high pressure and supercritical conditions

George Ebri *, Essa Alhashmi, Yasmine Baghdadi, Matyas Daboczi, Salvador Eslava, Klaus Hellgardt *

Department of Chemical Engineering, Imperial College London, South Kensington Campus, London SW7 2AZ United Kingdom

ARTICLE INFO

Keywords:
Cuprous oxide (Cu_2O)
carbon dioxide reduction (CO_2)
Photocatalysis
High pressure
supercritical CO_2
C-C coupling
Benzyl alcohol

ABSTRACT

Carbon dioxide (CO_2) utilization has received attention recently due to the negative impact of CO_2 in the environment. One promising way to use CO_2 is photocatalysis, in which light is used as a source of energy. However, photocatalysis is still very limited by low efficiency in the CO_2 reduction. Here, we report for the first time the simultaneous photocatalytic CO_2 reduction and benzyl alcohol activation under high-pressure and supercritical CO_2 using a combination of cuprous oxide (Cu_2O) and metallic copper (Cu^0) as a photocatalyst. The CO_2 photocatalytic reduction resulted in the formation of carbon monoxide (CO) as the main product. When using high-pressure CO_2, the production rate of CO was increased by 125 times compared to the low-pressure process. This production of CO was further improved (2.3 times) when applying supercritical conditions. This significant enhancement in the CO production rate resulted in nearly seven times higher CO production rate compared to the current state-of-the-art Cu_2O-based catalyst. When investigating the activation of benzyl alcohol, hydrobenzoin – the C-C coupling product – was identified as the main product (selectivity = 98 %). C-C coupling is highly attractive due to the challenges in obtaining these products through thermocatalysis. The process presented here has the potential to be applied using other photocatalysts in order to further enhance the CO production rate, offering a valuable alternative for CO_2 conversion.

1. Introduction

The increase of carbon dioxide concentration in the atmosphere has boosted the need for research related to CO_2 utilization [1–3]. The utilization of CO_2 to produce useful compounds can be achieved through photocatalysis [4,5]. These photocatalytic processes have their inspiration in photosynthesis, in which solar light is used by plants to transform CO_2 into chemical fuels [6]. Because of the opportunity to activate CO_2 using light, photocatalysis has attracted attention recently [7,8]. In the photocatalytic reduction of CO_2, the light is used to produce electrons and holes (charge carriers). The photogenerated electrons can participate in the CO_2 reduction and the holes in an oxidation reaction [6]. According to literature, CO_2 reduction has been mainly implemented in gas–solid and gas–liquid-solid reactors [9]. However, the photocatalytic activity of these processes is still low, facing important challenges related to process efficiency and photocatalyst stability [10,11].

Recent research studies have performed simultaneous CO_2 reduction and valorisation of organic compounds [12]. In these processes, the reaction is usually carried out by bubbling CO_2 in a liquid phase at atmospheric pressure and (simulated) sunlight is used as a source of energy. When illuminating the photocatalyst, the photogenerated electrons are used to reduce the CO_2 and the holes to oxidize an organic compound. The aim of this simultaneous activation is to improve the efficiency of the process by using the electrons provided by the organic compound and to produce organic valuable compounds for industrial applications [12]. Although this strategy can improve the production rate, the process is still limited by very low CO_2 solubility in the liquid phase at low pressures. The CO_2 solubility in the liquid phase can be increased by operating the reactor at high pressure which is expected to result in an enhanced photocatalytic activity. However, to date, simultaneous CO_2 activation and organic valorisation using photocatalysis in high-pressure and supercritical CO_2 has not been reported. To our knowledge there are only four previous reports that use high-pressure conditions to perform photocatalytic CO_2 reduction [13–16]. Two of these studies did not use any hydrogen source and still reported products with hydrogen like formic acid. The other two reports used water as

* Corresponding authors.
E-mail addresses: g.ebri21@imperial.ac.uk (G. Ebri), k.hellgardt@imperial.ac.uk (K. Hellgardt).

https://doi.org/10.1016/j.cej.2024.158356
Received 9 August 2024; Received in revised form 4 December 2024; Accepted 5 December 2024
Available online 3 January 2025
1385-8947/© 2024 The Author(s). Published by Elsevier B.V. This is an open access article under the CC BY license (http://creativecommons.org/licenses/by/4.0/).

electron donor and as a proton source. Using water presents three disadvantages: competition between CO_2 reduction and proton reduction to hydrogen, slow kinetics for water oxidation, and production of oxygen with low economic value [17]. Given these disadvantages, using organic compounds instead of water under high-pressure and supercritical CO_2 provides an opportunity to simultaneously improve the efficiency of the process and to produce high value products.

A key aspect of the photocatalytic process is the material used as a photocatalyst. Among the different photocatalysts used for CO_2 activation, copper-based materials offer important benefits, such as low material cost, non-toxicity and the possibility of activation by visible light [18]. Cuprous oxide (Cu_2O) is one of the most synthesized semiconductors in photocatalytic reactions and has been proven to reduce CO_2 under illumination [18–20]. More recently, adding metallic copper (Cu^0) to Cu_2O has been shown to increase the photocatalytic activity of this heterojunction [21–23]. However, these photocatalysts have not been tested under high pressure which has the potential to improve the photocatalytic activity when used for CO_2 reduction.

Another important part of the reaction is the choice of the organic compound to be activated simultaneously with the CO_2. One attractive compound is benzyl alcohol (BA) because it can be activated using photocatalysis [24–27], and it can be derived from biomass, making it obtainable from renewable resources [28]. The photocatalytic activation of benzyl alcohol has the potential to become a sustainable method for producing chemicals [29]. When activating benzyl alcohol using photocatalysis, the most commonly reported product was benzaldehyde (BD) which was produced by benzyl alcohol oxidation [29,30]. More recent studies have suggested that benzyl alcohol can be activated to enable C-C coupling, allowing the production of hydrobenzoin (HB), benzoin or other derived products [29,31,32]. This C-C coupling, obtained from the activation of C-H bond instead of C-O bond, is very challenging [33], and photocatalysis can offer a path to perform this reaction which is very difficult using thermocatalysis [28]. These compounds obtained from the C-C coupling reaction can be used as intermediates for the fine chemical production and the pharmaceutical industry [32]. When the simultaneous photocatalytic activation of benzyl alcohol and CO_2 has been performed at room temperature, the main reported product was benzaldehyde [34,35]. However, these reactions were performed under low pressure CO_2 which might have limited their performance due to the low CO_2 concentration in the liquid phase. Moreover, to date, benzyl alcohol and CO_2 activation has not been tested using supercritical CO_2 which might have a positive impact in the process efficiency.

In this study, we present for the first time the simultaneous photocatalytic CO_2 reduction and benzyl alcohol activation under high-pressure and supercritical CO_2. The use of high-pressure CO_2 had a remarkable impact in the photocatalytic activity which resulted in record-high CO production rate reported for Cu_2O-based photocatalysts. The obtained product from benzyl alcohol activation was the C-C coupling product of two benzyl alcohol molecules (selectivity = 98 %) which has not been reported before for this type of photocatalysts. This project provides a strategy to improve the efficiency of photocatalytic CO_2 activation by increasing the process pressure, paving the way for a sustainable CO_2 utilization.

2. Experimental section/methods

2.1. Chemicals

All chemicals were used without additional purification and stored according to recommendations. Benzyl alcohol (>99 % – BA) was purchased from Fluorochem. Copper acetylacetonate ($Cu(acac)_2$ – ≥99 %), fluorine tin oxide (FTO – 8 Ω/sq resistance) and hydrobenzoin (99 % – HB) were supplied by Sigma Adlrich, ethanol (99.8 %) by Fisher scientific, benzaldehyde (>99 % – BD) by Alfa Aesar and dimethylformamide (>99 % – DMF) by VWR.

2.2. Synthesis of photocatalyst Cu_2O and Cu_2O/Cu^0

The batch synthesis was performed following previous procedures [23,36]. The synthesis was conducted in a 100 mL three-neck flask equipped with a condenser to prevent solvent evaporation. Initially, BA (80 mL) was heated to 180 °C and maintained at this temperature for 10 min to ensure uniformity. Once the temperature stabilized, a solution containing 5.6 mmol of $Cu(acac)_2$ in 10 mL of BA was introduced into the heated BA. After allowing the reaction to proceed for the desired duration (30 – 150 min), the heating was stopped, and the flask was immediately cooled using an ice bath. Temperature was measured with a K-type thermocouple accurate to ± 2 °C. Upon completion of the reaction, the suspension containing the products was centrifuged three times at 4500 rpm for 20 min each, with the precipitates being washed with ethanol between each centrifugation. Finally, the resulting powder products were dispersed in ethanol using sonication and dried overnight in a vacuum oven at 60 °C for characterization and photocatalytic reaction.

2.3. Gas phase photocatalytic reaction

The CO_2 reduction in gas phase was carried out following previous reported procedure [37]. 10 mg of photocatalyst was dispersed homogeneously in a stainless-steel holder which was placed in a 20 mL cylindrical gas-tight stainless-steel photoreactor with a quartz window. DI water (40 μl) was placed inside the photoreactor to the side of the sample to saturate the atmosphere with H_2O, which was the electron donor for these experiments. The reactor was, then, evacuated with a vacuum pump to remove excess air and refilled with CO_2. The system was purged with CO_2 at 10 mL min^{-1} for 15 min after which the outlet and inlet of the photoreactor were closed and the system was left for 15 min to reach equilibrium between the photocatalyst and the gases. Once this time was finished, a 300 W Xe source (LOT-Quantum Design) equipped with an AM1.5G filter was used to simulate 1 sun (100 mW cm^{-2}) illumination. After 3 h, the gas phase was analyzed using a gas chromatography unit (Shimadzu Nexis GC-2030) equipped with a barrier ionization discharge (BID) detector coupled with a mass spectrometer (MS). For continuous flow measurements, the reactor inlet and outlet were kept open and constant CO_2 flow of 0.5 mL min^{-1} used to push the gas towards the injection port of the GC with samples taken every 20 min to be analyzed by the same GC-BID. For control experiments, CO_2 was replaced by argon.

2.4. Liquid-Gas phase photocatalytic reaction at low- and high-pressure CO_2

2.4.1. Setup for low- and high-pressure CO_2 reaction

The setup used to perform the photocatalytic reaction to activate BA and at different pressure of CO_2 is presented in Fig. S1. In this setup, the reactor was a homemade stainless-steel reactor with an inlet and an outlet, and a sapphire window (Rayotek – 101060) that can operate at high pressures and temperatures. To seal this window with the reactor body, a PTFE for gases was used. To ensure no leakages, the pressure of the reactor was monitored by using a pressure gauge (Omega) installed in the outlet of the reactor. The outlet of the reactor was connected to a vacuum pump to evacuate the system before the reaction, to the venting and to a gas tight bag (Supelco – Supel™) to perform the sampling of the gases. To stir during the reaction, a hot plate (IKA RCT basic) and stirring bar were used. The CO_2 inlet of the reactor was provided by a dip tube CO_2 cylinder (dip tube CO_2 cylinder CP grade – 111422-J). This inlet can be at low and high pressure. For the low-pressure operation, the outlet of CO_2 cylinder was heated to 50°C to transform the liquid CO_2 in gas CO_2 and then a regulator was used to reduce the pressure from the cylinder pressure (> 60 bar) to 3 bar monitored by another pressure gauge. This low-pressure CO_2 was fed to a mass flow controller (MFC) to control the flow rate of CO_2. This CO_2 flow was fed to the reactor after

evacuating the reactor and during purging the reactor with CO_2. The other CO_2 inlet was the high-pressure branch, whereby the liquid CO_2 was cooled down by an ice bath and feed to an HPLC pump (Gilson 307). The pump made possible to increase the pressure beyond the cylinder pressure to be able to achieve supercritical conditions. The outlet of the pump was fed to the reactor, usually after the purging process and before the start of the reaction. The high-pressure branch consisted of 1/8″ stainless-steel tubing. Selecting between the low or high-pressure inlet was done by a three-way valve. Once the reactor was ready for the reaction, a 200 W xenon lamp (Oriel instruments) was used as source of light adjusted to 240 mW cm^{-2}.

2.4.2. Setup operation for the photocatalytic reaction

In a standard procedure, the photocatalyst was first heated to 180°C in a vacuum oven to eliminate any remaining of the benzyl alcohol used during the synthesis and then dispersed in BA by sonication during 15 min. Once the photocatalyst was well dispersed, the suspension of BA and photocatalyst was placed inside the reactor with the stirring bar and the sapphire window was adjusted to seal the reactor. After closing the inlet of the reactor, a vacuum pump was used to evacuate the reactor to remove the oxygen from the system and the reactor was filled with CO_2. This evacuation of air and replacement by CO_2 was repeated 3 times. After this, CO_2 was bubbled through the solution of BA and the photocatalyst (120 mL min^{-1}) for 30 min to minimize the oxygen content in the system and in the solution. Once the bubbling time was finished, the outlet was closed. For low-pressure reactions, the inlet was the CO_2 coming from the MFC and the flow was on until reaching 3 bar of pressure (pressure of the low-pressure line). When high-pressure reaction was required, the three-way valve was changed to the high-pressure line, and the reactor was filled with high-pressure CO_2. For supercritical conditions, liquid CO_2 was pumped to increase the pressure, and the temperature was controlled by the hot plate under the reactor. After reaching the pressure and temperature required for the reaction, 10 min of wait time was implemented to equilibrate the reactant with the photocatalyst. Next, the xenon lamp was turned on and the reaction was started and maintained for 22 h. Once the time was completed, the light was turned off, and the products were centrifugated (4500 rpm – 20 min) to separate the photocatalyst from the liquid. The obtained solids were dispersed in ethanol for further characterization and the liquids were analysed using HPLC and GC. For HPLC analysis, (Shimadzu LC-2030C) a Gemini C-18 (Phenomenex) column was used and gradient between water and acetonitrile was implemented to obtain the separation. In the HPLC the products were detected using diode array detector (DAD). For GC (Shimadzu Nexis GC-2030), a low polarity column (Shimadzu SH-Rxi-5 ms) was used, and flame ionization detector (FID) and mass spectrometer (MS) were used to detect the products. To analyse the products in the gas phase, a gas-tight bag was connected to the end of the system and a vacuum pump was used to vacuum the line and the bag during 10 min. Then the bag was filled with the gas coming from the reactor. The gas products were analysed using a gas chromatograph (Shimadzu Nexis GC-2030) unit with a barrier ionization discharge (BID) detector and mass spectrometer (MS) (more details about the analytics in supplementary material Section S2).

2.5. Characterization

To characterize the crystalline structure and determine the composition of the obtained photocatalysts, X-ray diffraction (XRD) was performed using PANalytical Empyrean operated at 40 V and 40 mA as voltage and current of excitation source which was CuKα at 1.544 and 1.541 Å. The XRD spectra were obtained in the range of $2\Theta = 25 - 70°$, using 0.0167° as step and 60 s as time per step. The obtained patterns were compared with the reference PXRD patterns of Cu_2O (ICIDD no. 00-005-0667) and of Cu (ICIDD no. 01-071-4610).

Scanning electron microscopy (SEM) was implemented to characterize the morphology of the photocatalysts and the particle size using Zeiss Sigma 300, at 5 eV as accelerating voltage and 6 mm as working distance. After depositing the samples onto carbon tape, the samples were coated with chromium (Q150T Quorum – Layer = 15 nm) to improve the surface conductivity and reduce charging during the analysis. The particles were observed and measured in at least three different positions in the sample and at three different magnifications.

To confirm the oxidation state of the copper present in the synthetized photocatalysts, X-ray photoelectron spectrometry (XPS) was used. This analysis was implemented using a Thermo Fisher K-Alpha + instrument and a monochromated Al Ka micro-focused X-ray source. The patterns were corrected using C 1 s peak at 284.8 eV as a reference and Cu 2p and Cu LMM spectra were obtained using 40 scans.

Transmission electron microscopy (TEM) was conducted using TEM JOEL STEM 2100F operated at 200 kV. The sample was suspended in *iso*-propanol via sonification for 15 min. A drop was poured on carbon-coated copper grid and left to dry. The images were analysed using ImageJ to measure the lattice distances.

To analyse the light absorption of the different photocatalysts and to determine the band gap of the obtained semiconductor, UV–visible diffuse reflection spectroscopy (UV–Vis DRS − Shimadzu UV-2600) was employed. To perform this analysis, the absorbance of the different photocatalysts was measured in the visible range (400 – 800 nm) and barium sulphate ($BaSO_4$) was used as reference. The measured reflectance was used to obtain the Tauc plot to estimate the band gap of the photocatalyst [38].

Photocurrent measurements were obtained from a photoelectrochemical cell (PEC) using solar simulator (ABET Technologies − SUN 2000) adjusted at 1 sun as source of light. The used PEC was a standard three electrode setup. The working electrode was obtained by drop casting 100 µl of photocatalyst suspension in DMF with a concentration equal to 12.5 mg mL^{-1} on top of FTO-coated glass (15 × 15 mm) [22]. Before drop casting the photocatalyst suspension, the FTO was cleaned using DI water, acetone, and isopropanol. Platinum plate and silver/silver chloride 3 M electrode were used as counter and reference electrodes, respectively. The electrolyte was a solution of 1 M of Na_2SO_4 stirred previously during 20 min with nitrogen [39]. The current was measured fixing the potential at −0.4 V vs. silver/silver chloride reference electrode using a potentiostat (Nanoelectra NEV 4). The light was turned on and off every 10 s using a shutter in order to obtain the photocurrent.

Photoluminescence (PL) measurements (FLS1000-Edinburgh Instruments) were performed to check the improved charge separation when adding small amount of Cu^0 to the photocatalyst. Xenon arc lamp (450 W, ozone free) was used as light source to generate the excitation source at 450 nm with a bandwidth of 10 nm and a longpass filter with 495 nm cut-off wavelength was used before the detector.

To determine the workfunction of Cu_2O and Cu^0, Kelvin probe (KP Technology, SKP5050) measurements were performed. The workfunction of the tip was calibrated using a freshly cleaned silver reference. To determine the valence band edge position of Cu_2O, ambient-pressure photoemission spectroscopy (APS) was used, scanning UV light irradiation (4.2 – 5.8 eV) and extrapolating the cube root photoemission to zero. These measurements were performed using a thin uniform layer layers of the powders deposited on indium-doped tin oxide (ITO)-coated glass substrates.

3. Results and Discussion

3.1. Synthesis of Cu_2O/Cu^0 and characterization

This section describes the synthesis and characterization of the Cu_2O/Cu^0 photocatalyst obtained by reducing $Cu(acac)_2$ as precursor and BA as solvent and reductor. First, Cu_2O is obtained as a product of the reduction of copper salt. Further reduction produces Cu^0 [36]. This sequential production of Cu^0 from Cu_2O can enable the control of the ratio of Cu^0 and Cu_2O in order to optimize the photocatalytic activity of

this photocatalyst. Consequently, the synthesis was performed at 180°C and different reaction times were implemented in order to control the ratio of Cu^0 and Cu_2O. To confirm this control between Cu_2O and Cu^0, XRD analysis was performed in the synthetized photocatalysts at different reaction times. To determine the presence of Cu_2O and Cu^0 using XRD, peaks at 36.4° and 42.6° were evaluated, respectively. As presented in Fig. 1a, at reaction times of 50 min or shorter, the peak at 36.4° was obtained and no peak at 42.6° was detected. This result indicated that for synthesis carried out at reaction times shorter than 50 min, the only obtained product was Cu_2O. When increasing the reaction to 100 min or higher, Cu^0 peak at 42.6° was detected. The presence of this peak confirmed that a mixture of mainly Cu_2O and small amounts of Cu^0 was obtained. Further increase in the reaction time to 150 min, produced higher amounts of Cu^0.

To confirm that, as shown by XRD, the obtained photocatalyst was a combination of Cu_2O and Cu^0 and that CuO was not present, XPS was implemented. CuO can be identified by the presence of a pronounced shake-up satellite in the Cu 2p spectra, occurring at a binding energy range of 940–944 eV [40]. As illustrated in Fig. 1b, there was no strong satellite around 943–944 eV for both samples obtained at reaction time equal to 30 and 100 min. The lack of detection of the strong satellite suggested the absence of CuO and confirmed that the photocatalyst was a combination of Cu_2O and Cu^0. The Cu LMM was also used to confirm that the catalyst was a combination of Cu_2O and Cu^0 (Fig. S26).

SEM was used to characterize particle morphology, and the results are presented in Fig. 2a-b. The particles were mainly cubes in the case of Cu_2O obtained at 30 min as reaction time. When increasing the reaction time to 100 min, larger cubes were obtained, and small spheres of 22 nm were detected on the cubes surface (Fig. S24). These small spheres are assigned to Cu^0 nanoparticles obtained as a product of the Cu_2O reduction. The obtained photocatalyst was also characterized using TEM (Fig. 2c-d) where cubes with small spheres were also detected. When analysing the particles at high magnification, lattice fringes were observed confirming the crystalline structure detected in XRD. The distance between these lattice fringes was measured in the TEM images as illustrated in Fig. 2e-f (Fig. S25). The lattice distance in the cubes was 2.46 Å, assigned to the (1 1 1) crystallographic plane of Cu_2O. The small spheres presented 2.02 Å lattice fringes, assigned to the (1 1 1) crystallographic plane of Cu^0. This lattice spacing confirmed the presence of a combination of Cu_2O and Cu^0.

To characterize the light absorption of the obtained photocatalyst, UV–Vis diffuse reflectance spectroscopy was used (Fig. 3a). When reducing the photocatalyst to produce small amounts of Cu^0, the light absorption was improved in the visible range mainly because of the peak related to Cu^0 around 600 nm which is related to the surface plasmon resonance effect of Cu [41,42]. These results were also used to estimate the bandgap of the Cu_2O nanoparticles as presented in Fig. S10. The obtained bandgap was 2.02 eV which is in good agreement with the literature [39]. To characterize the photocatalytic activity of this material, photoelectrochemical (PEC) measurements were performed. In this experiment, a constant potential was applied, and the light was chopped at regular intervals of 10 s. When turning on the light, the current increased due to the generated electrons and holes. The difference between the current density in dark and under illumination is the photocurrent density, which confirms the photocatalytic activity of the analysed material. As shown in Fig. 3b, the photocatalyst containing a small amount of Cu^0 presented higher photocurrent density compared with pure Cu_2O. When the Cu^0 content was further increased, the photocurrent started to decrease due to the reduced light absorption by the smaller amount of Cu_2O. This behaviour where the photocurrent initially increased with a small amount of Cu^0 and then decreased at higher amounts of Cu^0 suggested a competition between the photogeneration of electrons and holes with the recombination of these charge carriers. Therefore, when introducing small amounts of Cu^0, the recombination rate of electrons and holes is expected to be reduced due to enhanced charge carrier separation, without much impact on absorption and charge carrier generation. However, at higher amounts of Cu^0 the photoexcitation of electrons is reduced and not be compensated anymore with the reduced recombination, resulting in the observed reduction of photocurrent. To confirm the enhanced charge carrier separation, photoluminescence (PL) measurements were carried out in samples with different ratio of Cu_2O and Cu^0. The PL emission occurs due to the radiative recombination in Cu_2O. The quenching of the PL signal is often related to enhanced charge separation reducing the radiative recombination of the photocatalyst [43,44]. As observed in Fig. S11, the PL intensity was reduced when increasing the amount of Cu^0 confirming the positive impact of Cu^0 on charge carrier separation, in agreement with the literature [22]. Therefore, the incorporation of small amounts of Cu^0 reduced the recombination rate by improving charge carrier separation, without affecting the photogeneration of charge carriers. However, as discussed before, after further increasing the amounts of Cu^0 beyond the optimum point, the photocurrent decreased due to the reduction in the charge generation.

Next, the charge carrier dynamics at the Cu_2O/Cu^0 interface was investigated and for this the position of the Fermi level, and valence and conduction band edges of Cu_2O were determined. These measurements are carried out in an air atmosphere and because of this they might better represent the behaviour of the material during gas phase reaction compared to liquid reactions. Despite this limitation, these measurements are still a good reference to understand the flow of the charge carriers in the photocatalyst when illuminated. In order to determine this, the work function of both Cu_2O and Cu^0 were measured by Kelvin probe. As shown in Fig. 3c, Cu^0 presented a smaller work function (and so shallower Fermi level) compared to Cu_2O. The valence band edge of

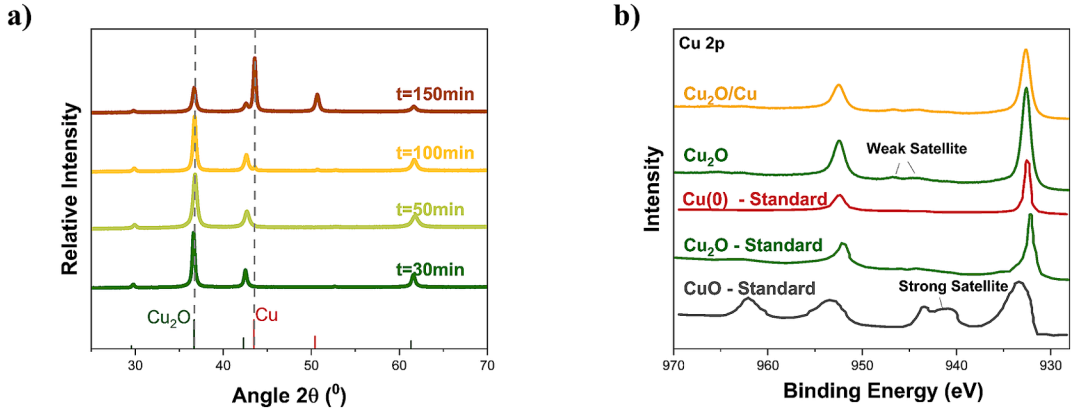

Fig. 1. a) X-ray diffractograms of the particles obtained at 180 °C and different reaction times. b) XPS spectra of Cu_2O (temperature 180 °C and reaction time 30 min) and Cu_2O/Cu^0 (temperature 180 °C and reaction time 100 min). Standards of CuO, Cu_2O and Cu^0 were added from Biesinger et al [40].

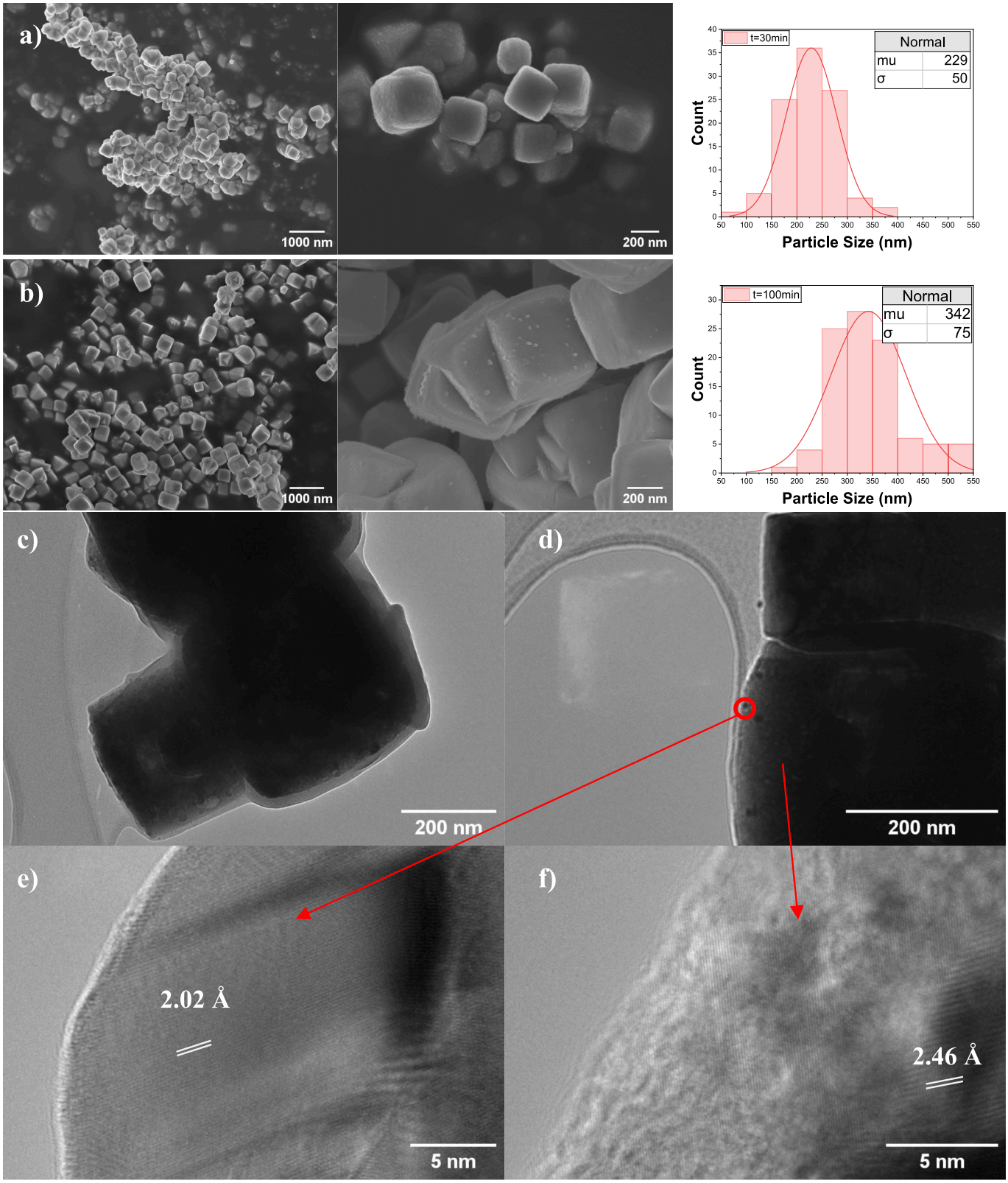

Fig. 2. a) SEM micrographs and particle size distribution of Cu_2O, obtained at 180 ℃ and 30 min as reaction time. b) SEM micrographs and particle size distribution of Cu_2O/Cu^0, obtained at 180 ℃ and 100 min as reaction time. c-d) TEM images for Cu_2O/Cu sample obtained at 180 ℃ and 100 min as reaction time. e-f) Lattice spacing measurements obtained from the TEM micrographs after processing the image through ImageJ for e) Cu and f) Cu_2O (Details in Fig. S25).

Cu_2O was determined at around −4.8 eV by ambient photoemission spectroscopy (Fig. 3d). The distance between the valence band edge and the fermi level was also confirmed using XPS (Fig. S28). By considering the position of valence band edge and the bandgap obtained from UV–Vis spectroscopy, the position of the conduction band edge of Cu_2O was calculated. The energy levels of Cu_2O and Cu^0 are illustrated in Fig. 3e and are in good agreement with previous reports [45]. As can be observed, the conduction band edge obtained from Cu_2O was more

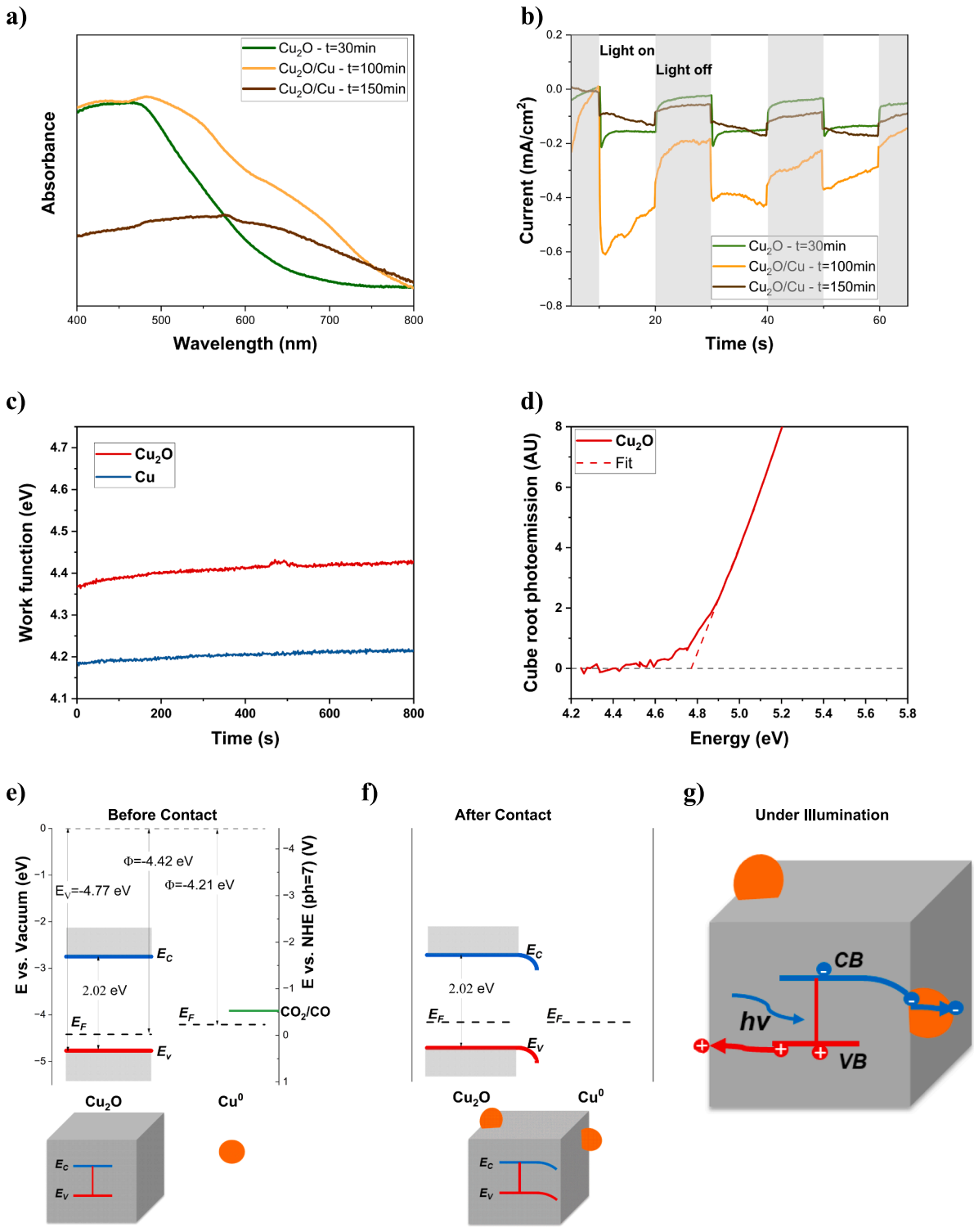

Fig. 3. a) UV–Vis diffuse reflectance measurements done in the photocatalyst synthetized at 180 °C and at different reaction times, containing different proportions of Cu_2O and Cu. b) Photocurrent measurement carried out in a PEC with, maintaining the potential constant at −0.4 V vs. Ag/AgCl and turning on and off the light by intervals of 10 s as shown in the chart, for photocatalyst containing different proportions of Cu_2O and Cu. c) Stable work functions obtained by Kelvin probe measurements for Cu_2O and Cu. d) Ambient pressure photoemission spectroscopy used to estimate the valence band edge of Cu_2O. e) Fermi level (E_F) position of Cu^0 and Cu_2O, and valence band (VB) and conductive band (CB) edges obtained from kelvin probe, photoemission spectroscopy and UV–Vis diffuse reflectance spectroscopy measurements before contact. f) Band alignment and band bending after Cu^0 and Cu_2O are in contact. g) Scheme of charge transfer when Cu_2O/ Cu^0 is illuminated.

negative than the potential needed to reduce CO_2 towards CO, and this was also confirmed by measuring the valence band edge of the composite Cu_2O/Cu^0 (Fig. S29). After forming electrical contact in dark between Cu_2O and Cu^0, the Fermi levels are aligned [46] (Fig. 3f). As the work function of Cu^0 was smaller than Cu_2O, the Fermi level alignment resulted in band bending (*i.e.*, electric field) which helped the transport of photogenerated electrons from Cu_2O towards Cu^0 [5]. Therefore, when the photocatalyst was illuminated, the generated electrons

migrated to Cu^0 which resulted in an improved separation and reduced recombination of charge carriers (Fig. 3g). Once these electrons reached the surface of Cu^0, they can participate in a reduction reaction and the holes left in Cu_2O can participate in an oxidation reaction. The enhanced separation of photogenerated electrons and holes expected based on the energy level measurements is in good agreement with the reduced PL intensity and improved PEC performance discussed above. This enhanced charge separation reflects the behaviour of the fresh photocatalyst, whose composition may evolve over time, thereby altering the dynamics of the charge carriers.

To test the photocatalytic activity for CO_2 reduction of this photocatalyst, a gas phase reaction was performed in a CO_2 atmosphere and water was used as electron donor. First, a continuous reaction was performed where H_2 concentration was measured by sampling every 20 min for the Cu_2O and Cu_2O/Cu^0 photocatalysts to determine the time of maximum production rate (Fig. S12). Based on these experiments, 3 h was selected as reaction time. The CO and H_2 concentrations were measured at the beginning and at the end of the reaction to calculate their production rate. These productivities of CO and H_2 obtained as products of the reaction are presented in Fig. 4a. To confirm that CO was produced from the CO_2 reduction and to discard other sources of CO, a control experiment was implemented under the same reaction conditions, but CO_2 was replaced by argon. As can be seen in Fig. 4a, no CO was detected at the end of the control experiment, confirming that CO was produced by the CO_2 reduction. When comparing the production rate of CO, Cu_2O/Cu^0 produced almost 6 times more CO than the bare Cu_2O. This enhanced production rate was due to the better electrons and holes separation of the Cu_2O/Cu^0 junction as suggested by the photocurrent and photoluminescence experiments. These results confirmed that Cu_2O/Cu^0 was able to reduce CO_2 and that adding small amounts of Cu^0 to the catalyst improved its photoactivity as suggested by previous reports [22].

3.2. Photocatalytic performance

Once the Cu_2O/Cu^0 was characterized and tested for CO_2 reduction, the next step was to perform the photocatalytic reaction of CO_2 and benzyl alcohol. This reaction was performed at low (3 bar) and high pressure (60 bar) to investigate the impact of this variable on the production rate and selectivity. After finishing the reaction, the liquid and gases were collected to be analysed using HPLC and GC respectively as explained in the experimental section. In the first part of this section, the production rate results will be presented and discussed. After that the mechanism of the reaction will be analysed and discussed based on the control experiments performed.

3.2.1. Photocatalytic reaction for CO_2 reduction and benzyl alcohol activation

The simultaneous CO_2 and BA activation was performed at low- and high-pressure CO2, using the synthetized Cu_2O and Cu_2O/Cu^0 photocatalysts. The photocatalyst was first dispersed in pure benzyl alcohol and then the system was evacuated and filled with CO_2. After 22 h of

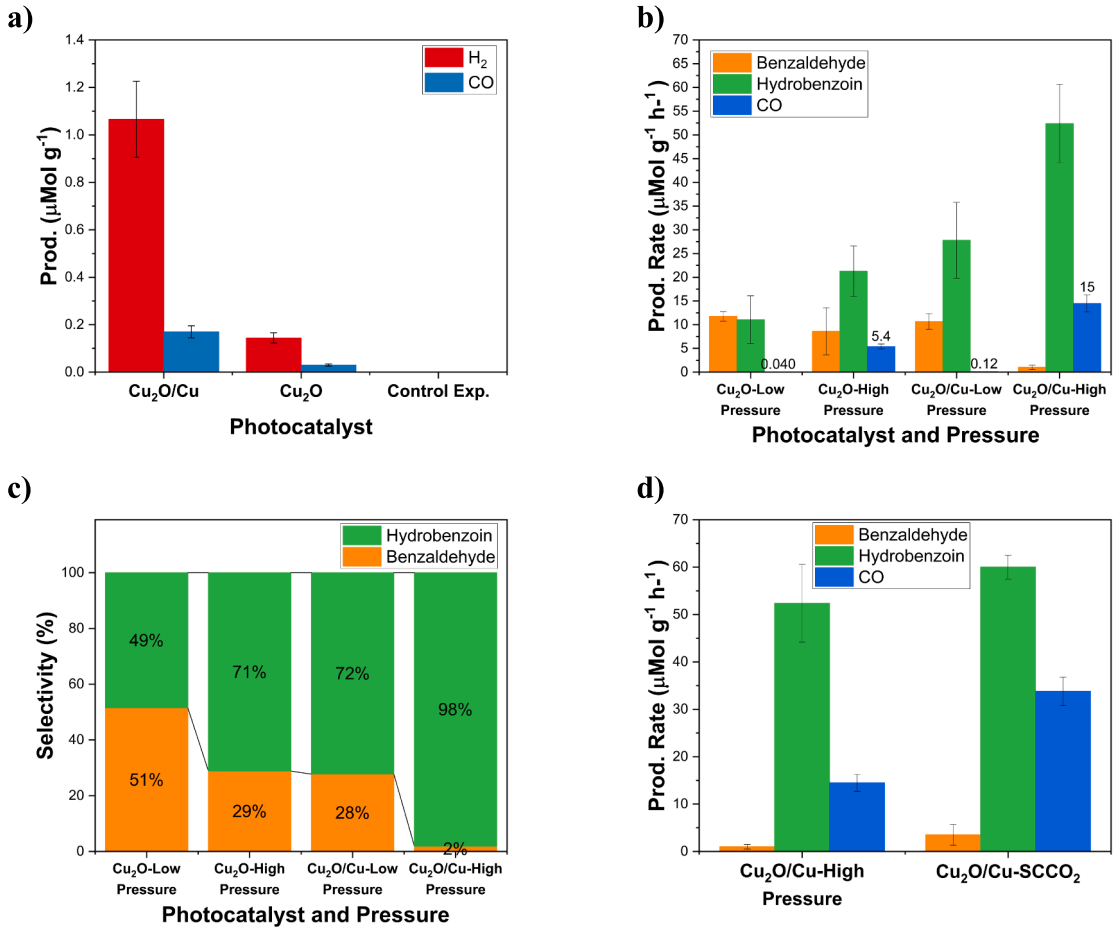

Fig. 4. a) CO and H_2 production rate as µmol g^{-1} for Cu_2O/Cu^0 and Cu_2O catalyst measured after 3 h of photocatalytic reaction in gas phase under illumination. Control experiment carried out at same conditions without CO_2 and H_2O. b) Production rate in µmol $g^{-1}h^{-1}$ and c) Selectivity of benzaldehyde, Hydrobenzoin and CO obtained using different photocatalysts and pressure of CO_2. Low pressure = 3 bar. High pressure = 60 bar. d) Comparison of the production rate of benzaldehyde, hydrobenzoin and CO obtained under higher pressure and supercritical CO_2. High pressure = 60 bar. $SCCO_2$ = 78 bar and 70 °C.

reaction under light, the liquid was analysed using HPLC. The main detected products were benzaldehyde (BD) and hydrobenzoin (HB) which is the coupling product of two benzyl alcohol (BA) molecules. As can be seen in Fig. 4b, when increasing the pressure of CO_2, in both Cu_2O and Cu_2O/Cu^0 photocatalysts the production rate of HB increased, and the production of BD decreased. However, the Cu_2O/Cu^0 improved the HB production by 2.5 times when compared with the bare Cu_2O at high pressure. Another key aspect was that the selectivity improved from 71 to 98 % making HB the main product (Fig. 4c).

When analysing the gas products, CO and H_2 were detected. Following the same trend as in gas phase reaction, when introducing small amounts of Cu^0, the production of CO was enhanced (Fig. 4b). When implementing high pressure, the production rate of CO was increased by 120 times compared with the low-pressure process. To verify that CO was produced by the CO_2 reduction, and it was not the product of BA decomposition, a control experiment was performed. In this control experiment, the same reaction conditions were implemented but without the photocatalyst. As can be seen in Fig. S14, no CO was detected under these conditions, which confirmed that CO_2 and the catalyst were needed to produce CO. This result confirmed what was obtained during the gas phase reaction as discussed in section 3.1, where CO was only produced when both the photocatalyst and CO_2 were present in the reaction. In the same control experiments, the liquid was analysed, and no HB was detected (Fig. S15). Moreover, another control experiment using argon atmosphere instead of high-pressure CO_2 showed no HB and no CO products after 22 h of illumination. When performing the reaction without light, no products were detected. These experiments confirmed that the photocatalyst, light and CO_2 were needed to produce HB and CO.

Based on these results, where CO was obtained only when catalyst, light and CO_2 were used in the reaction media in two different setups and using two different electron donors, it can be concluded that the CO was a result of the CO_2 photocatalytic reduction. These results also indicated that CO_2 and benzyl alcohol were activated separately as suggested in previous reports [47–49].

When implementing supercritical CO_2 by increasing the temperature (70 °C) and the pressure (78 bar), the production rate of CO and HB were increased (Fig. 4d). This enhancement in the photoactivity suggests that CO_2 plays an important role in the photocatalytic activation. First, CO_2 might be extracting the generated electrons from the photocatalyst when illuminated resulting in a higher availability of holes for the BA activation. These holes might oxidize BA and the electrons reduce CO_2 to produce CO. In this way the production of CO was doubled when compared to high-pressure CO_2 reduction. Therefore, when using supercritical CO_2, the extraction of electrons might be improved resulting in a better charge carrier separation. This improvement in the charge carrier separation may enhance the production rate for both CO_2 reduction and BA activation.

3.2.2. Control experiments and reaction mechanism

Once the liquid and gas products of the photocatalytic reaction were analysed, the next step was to determine the reaction mechanism. In order to unveil the reaction mechanism for the simultaneous CO_2 and BA activation and to investigate the stability of the photocatalyst, first the remaining photocatalyst after the reaction was characterized. This characterization is very important to understand the role played by the photocatalyst and to determine if there were any changes in the oxidation state of the copper. Because of this, the remaining photocatalyst after the reaction was investigated using XRD, XPS and SEM to determine any composition and morphology differences from the initial state. As can be seen in Fig. 5a, the XRD showed that the peak related with Cu^0 was not present after the photocatalytic reaction. This absence of the Cu^0 indicated that during the reaction metallic copper might have been oxidized. To further investigate the photocatalyst, SEM was performed in the samples. In this analysis, the cubes were still present but small spheres were detected in the cubes surface. These SEM images suggested the formation of a new material layer on top of the Cu_2O (Fig. 5c-d). Finally, to determine the surface composition, XPS was performed onto the used photocatalyst. The XPS analysis (Fig. 5b) showed strong satellites for Cu^{2+} which were not present in the fresh photocatalyst. This result confirmed that copper was oxidized during the reaction to form CuO. This change in the copper oxidation states might modify the flow of the charge carriers in the photocatalyst. To obtain this CuO, an oxygen atom was needed which might come from the CO_2 reduction. To further confirm that the oxidation of the photocatalyst was because of the CO_2, the reaction was performed using argon as atmosphere instead of high-pressure CO_2 and the remaining photocatalyst was characterized using XPS. In the XPS analysis (Fig. 5b), no satellite for CuO were detected confirming that the presence of CO_2 in the reaction environment was necessary for the copper oxidation. The remaining photocatalyst after the reaction under argon atmosphere was also characterized using XRD to determine if Cu^0 was still present in the material composition (Fig. 5a). The Cu^0 peak at 42.6° presented a higher relative intensity, showing that the amount of Cu^0 was increased after the reaction which is in agreement with previous literature where Cu_2O was reduced to produce copper under light [50]. This increase in the amounts of Cu^0 suggested that Cu_2O was reduced during illumination to Cu^0 which is plausible to be a result of the absence of species that can consume the generated electrons such as CO_2. As no CO_2 was present in the reaction environment, the generated electrons were not able to participate in a reduction reaction, which resulted in a reduction of Cu_2O to Cu^0. By comparing the oxidation state of the photocatalyst at the end of the photocatalytic reaction under argon and CO_2, it can be concluded that the oxidation of copper to CuO was produced by the presence of CO_2 during the photocatalytic reaction. During the reaction, CO_2 was reduced to CO by consuming the generated electrons and Cu^0 might have been oxidized by the produced holes and the remaining oxygen from the CO_2 reduction (**Eqs. (2)-(3)**).

Once the photocatalyst was characterized, control experiments were performed in order to determine the reaction mechanism for hydrobenzoin formation (Table S2). In these experiments, hole scavengers (triethanolamine) [24], electron scavenger (nitrobenzene) [30,51] and O_2^- scavenger (benzoquinone) [30] were used to understand the reaction mechanism.

As illustrated in Fig. S16, when using hole scavenger triethanolamine, the production of benzaldehyde and hydrobenzoin were suppressed. This result suggested that holes were needed for the benzyl alcohol activation as reported in literature [29,30]. The holes might participate by activating the C-H and O-H bonds according to the **Eqs. (4)**. In this way, holes can take the electrons from the mentioned bond and produce benzaldehyde by releasing two protons. The holes might also participate in C-H activation, by releasing a proton and a radical with on electron in the carbon. These radicals may react and produce the coupling product which was hydrobenzoin. To determine if benzaldehyde was only produced by holes and not by the presence of O_2 in the system, benzoquinone was used to trap O_2^- radicals (Fig. S18). In this experiment, benzaldehyde was produced confirming that holes were only involved in the benzaldehyde formation and O_2 was not part of the benzyl alcohol oxidation. This result confirmed that evacuating the system and purging with CO_2 was an effective way to reduce to a minimal the O_2 concentration and to suppress the O_2 effect in the benzyl alcohol oxidation.

To further investigate the reaction mechanism, a reaction was performed using nitrobenzene as an electron scavenger. The electron scavenger suppressed the CO production (Fig. S14). This suppression in the CO formation confirmed that CO was formed by the CO_2 photocatalytic reduction, as it was also observed in the results obtained in the previous experiments. When analysing the liquid products, benzaldehyde was produced but no hydrobenzoin was detected (Fig. S16). This suppression in the HB production can be explained by two potential causes: either by the absence of CO_2 reduction which might have been needed in order to produce hydrobenzoin; or because electrons might

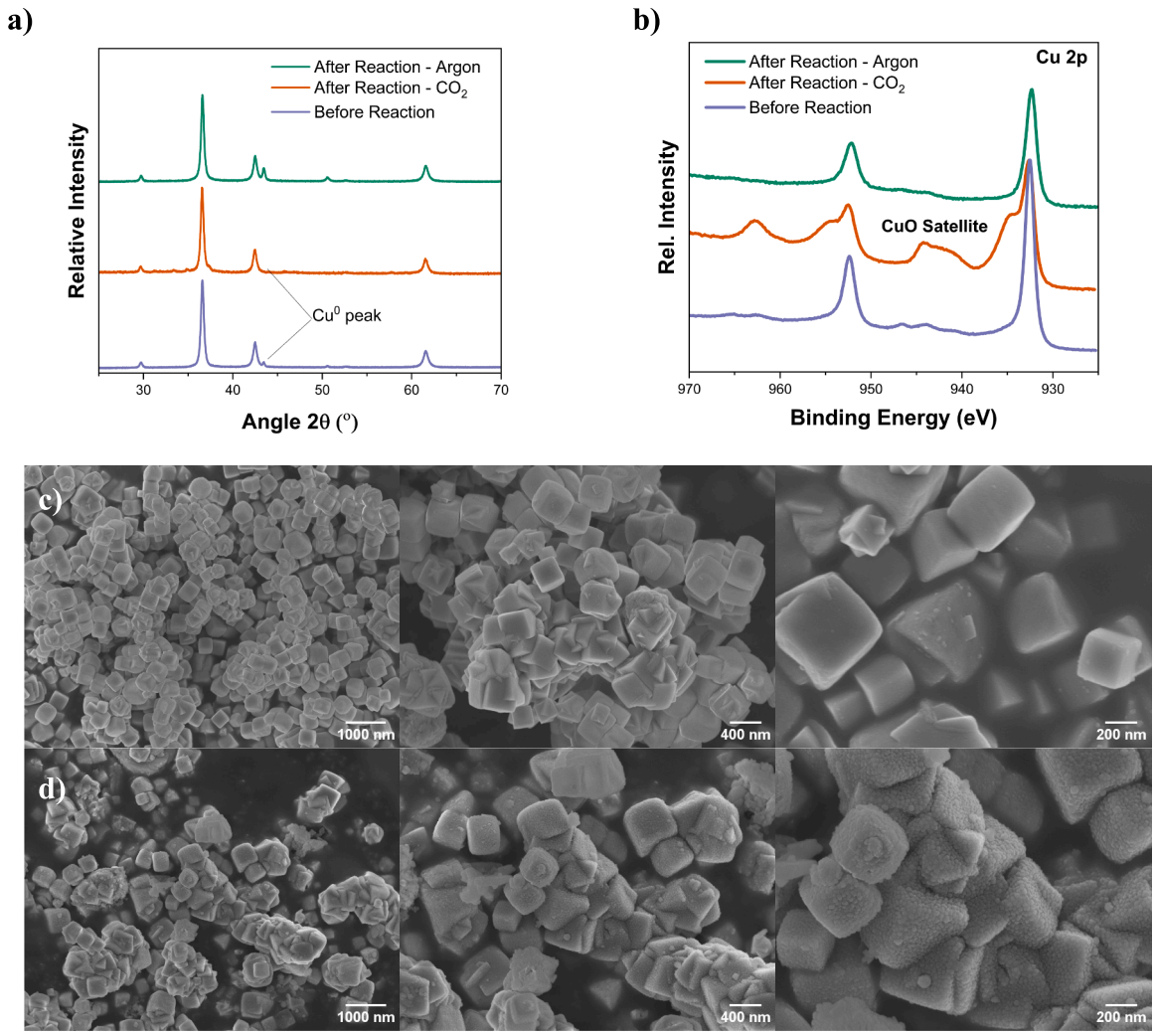

Fig. 5. Characterization of the photocatalyst before and after the reaction under CO_2 and argon atmosphere using a) XRD and b) XPS – Cu 2p. SEM images of the nanoparticles at different magnifications c) before the reaction and d) after the reaction.

participate in the production of hydrobenzoin, and they were no longer available due to the presence of nitrobenzene.

The first option where the reduction of CO_2 was needed for the hydrobenzoin production is supported by the result obtained when using argon instead of CO_2. In this case, no hydrobenzoin was produced and the photocatalyst was reduced to Cu^0 (Fig. S15). Furthermore, the formation of hydrobenzoin was also higher using high-pressure CO_2 in the photocatalytic process. Therefore, the reduction of CO_2 might promote the production of hydrobenzoin. This positive impact in the hydrobenzoin formation can be explained by the improved electron extraction when CO_2 was reduced and by the change in the oxidation state of the photocatalyst when performing the reaction. As discussed before, the copper was oxidized to produce CuO while reducing CO_2. This newly formed CuO can provide holes at higher oxidation potential, which can participate in the activation of C-H of the benzyl alcohol molecule.

The other possibility to explain the formation of hydrobenzoin, was suggested by Han et al in which electrons might participate in the formation of the coupling product by activating benzaldehyde [31]. In this case, once the benzaldehyde was formed, the C=O bond might be activated by electrons and protons to produce a radical which can react with benzyl alcohol to produce hydrobenzoin. To test this hypothesis, benzaldehyde was added to the reaction environment and as can be seen in Fig. S20, the production of hydrobenzoin was highly increased. Therefore, by taking both alternatives for the hydrobenzoin formation, hydrobenzoin is likely to come from the holes when activating benzyl alcohol or from electrons when benzaldehyde started to be present in the reaction environment. However, the high increase in the hydrobenzoin production when adding benzaldehyde indicated that the path in which electrons were used to reduce benzaldehyde and produce hydrobenzoin is likely to be the predominant one. To perform a deeper analysis in both pathways and to validate the radicals formation under the high pressure CO_2 conditions, in-situ analysis may be required. However, due to the challenges of working under high pressure, this analysis was not performed, leaving an opportunity for future research.

Taking these results into account, a mechanism can be proposed (Fig. 6c). When illuminating the photocatalyst, electrons can flow to Cu^0, improving the charge separation as suggested by the analysis of charge carrier dynamics. The electron flow from Cu_2O towards Cu^0 was confirmed by the measurement of the workfunction of both materials, the improved photocurrent and PL results and more importantly by the improvement in the photocatalytic reaction towards CO obtained in the gas phase reaction and in the liquid phase reaction at low- and high-pressure conditions. These electrons are likely to participate in the CO_2 to produce CO (**Eqs. (2)**). During the formation of CO, the photocatalyst was oxidized to produce CuO. The layer of CuO might generate holes at higher oxidation potential that can oxidize benzyl alcohol to produce benzaldehyde (**Eqs. (4)**) and activate the C-H bond of benzyl alcohol to produce radicals which can combine to produce

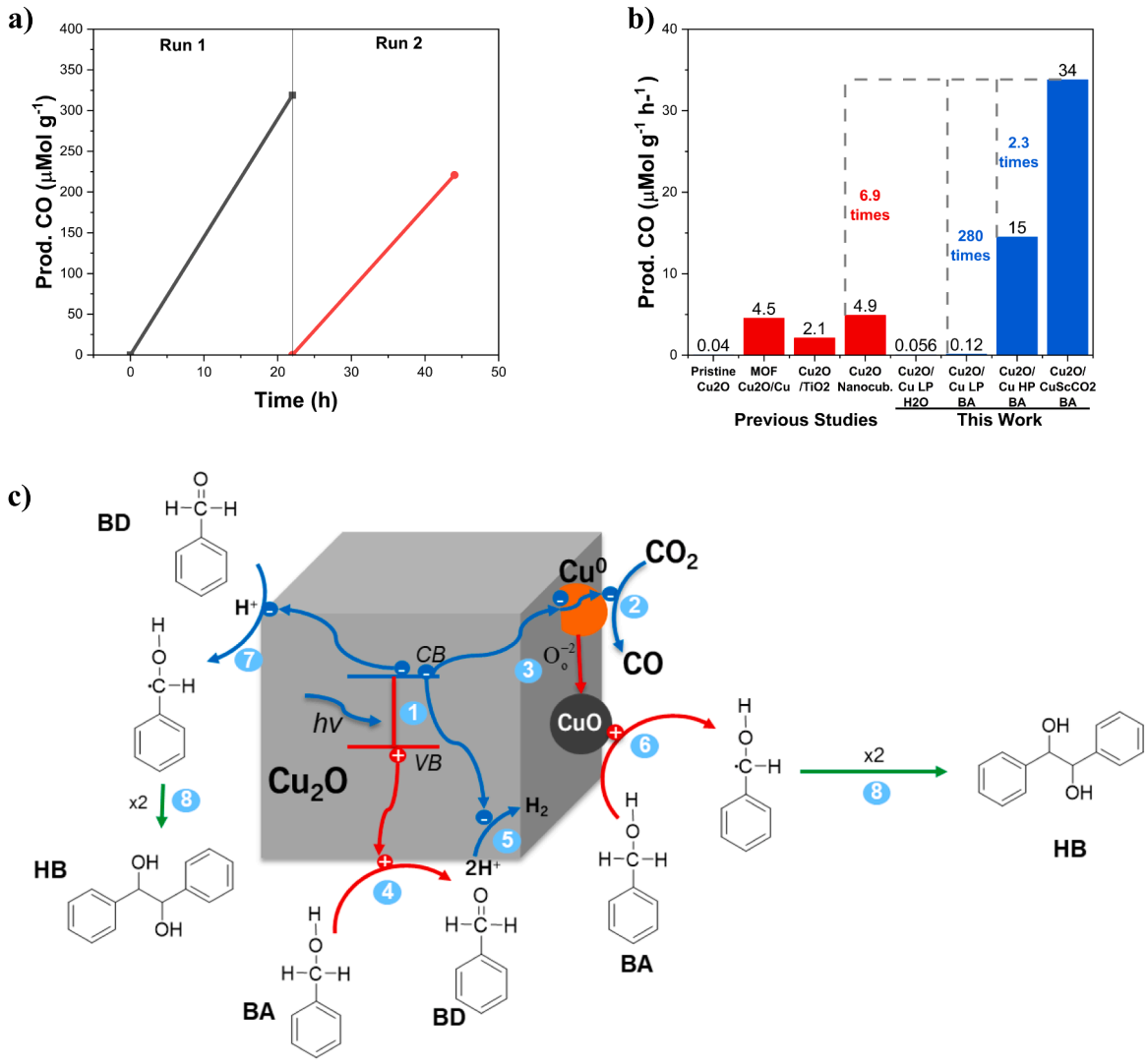

Fig. 6. a) Production of CO obtained for fresh (run 1) and used (run 2) photocatalyst. b) Comparison of CO production rate with previous studies (reproduced from [20]) and the different test conditions performed in this study for Cu_2O/Cu^0 photocatalyst: LP = Low pressure CO_2, HP = High pressure CO_2, H_2O = water, BA = Benzyl alcohol, $ScCO_2$ = supercritical CO_2 [19,20,56,57]. More information in **Table S3**. c) Scheme of the proposed reaction mechanism including the possible reaction paths. BA: benzyl alcohol, BD: benzaldehyde, HB: Hydrobenzoin. The number presented in each reaction are the number of the reaction equations.

hydrobenzoin (**Eqs. (6)-(8)**). The formation of hydrobenzoin by radicals was also supported by the detection of two isomers of hydrobenzoin when analysing the products (supplementary material Section S2.4). The formed benzaldehyde can be activated as well by the generated electrons in C-H bond to produce hydrobenzoin as final product (**Eqs. (7)-(8)**) which is likely to be the predominant path of hydrobenzoin formation. The protons released by the oxidation of benzyl alcohol or from the coupling product might take electrons and evolve to produce hydrogen which was detected in low amount compared with the other products (Fig. S13).

Step 1. Charge generation by photoexcitation.

$$Cu_2O \xrightarrow{Light} e^- + h^+ \quad (1)$$

Step 2. CO2 reduction and photocatalyst oxidation.

$$CO_2 + 2e^- \rightarrow CO + O_o^x \quad (2)$$

$$Cu^0 + 2h^+ + O_o^{-2} \rightarrow CuO \quad (3)$$

Step 3. Benzyl alcohol Oxidation to benzaldehyde and Hydrogen Formation.

$$C_6H_5CH_2OH + 2h^+ \rightarrow C_6H_5CHO + 2H^+ \quad (4)$$

$$2H^+ + 2e^- \rightarrow H_2 \quad (5)$$

Step 4. Hydrobenzoin formation from benzyl alcohol and benzaldehyde.

$$C_6H_5CH_2OH + h^+ \rightarrow C_6H_5C^{\cdot}HOH + H^+ \quad (6)$$

$$C_6H_5CHO + e^- + H^+ \rightarrow C_6H_5C^{\cdot}HOH \quad (7)$$

$$2C_6H_5C^{\cdot}HOH \rightarrow C_{14}H_{14}O_2 \quad (8)$$

To determine if the photocatalyst was still active at the end of the reaction (22 h), an experiment with a double reaction time (44 h) was implemented. In this reaction, the production rate of hydrobenzoin was higher when compared with the 22 h experiment and the production rate of CO remained almost constant (Fig. S17). This constant activity

after 44 h suggested that the photocatalyst was still very active after the first reaction of 22 h. To confirm the activity of the photocatalyst at the end of the reaction, an additional reaction employing the used photocatalyst was performed. When taking the used photocatalyst and dispersing it again in benzyl alcohol to perform the second run, the production rate of CO decreased as can be seen in Fig. 6a. This decrease in the CO production rate can be explained by the change in the oxidation state of Cu^0 to CuO and the formation of a CuO layer on the photocatalysts surface as demonstrated by the XPS analysis. This change in the oxidation state of metallic copper is likely to reduce the number of active sites for CO_2 reduction, consequently reducing the photocatalytic activity of this photocatalyst. Moreover, the layer of CuO that was formed during the first use of the photocatalyst is plausible to reduce its capacity to receive an oxygen atom during CO_2 reduction. However, it is important to highlight that the photocatalyst was still active to produce CO which agrees with the literature where Cu_2O can participate in the CO_2 reduction to produce CO [52]. Another aspect is the role of Cu^0, which acted as an electron acceptor and participated in the CO_2 reduction. However, as the CO_2 reduction still occurred in the second run, it can be concluded that the Cu plasmon resonance effect was not the predominant effect in the reaction performance. More cycling of the photocatalyst was not performed due to limitations in the photocatalyst recovery after the first cycle.

On the other hand, when analysing the production rate towards hydrobenzoin, this CuO formation can increase the oxidation potential of the generated holes as CuO presents a lower valence band edge than Cu_2O [53–55]. This increase in the oxidation potential of the holes is expected to improve the benzyl alcohol oxidation, resulting in a better production rate towards HB as illustrated in Fig. S19. This improvement in the photocatalyst activity towards hydrobenzoin suggested that the generated electrons were more likely to produce hydrobenzoin instead of CO.

Another important aspect of understanding the nature of the photocatalytic reaction was testing the reaction under different light sources. To implement this, the benzyl alcohol activation was performed using two led lights with wavelengths equal to 365 and 455 nm (Fig. S27). In both experiments the main products of benzyl alcohol activation were benzaldehyde and hydrobenzoin showing that the reaction occurred under UV and visible light.

3.2.3. *Improving photoactivity and comparison with literature*

The aim of this section is to compare the production rate obtained under different process conditions and perform a comparison with previous studies. The Cu_2O/Cu^0 presented a better performance than the bare Cu_2O as discussed before. Because of this, the comparison was performed using Cu_2O/Cu^0 photocatalyst under different reaction conditions. The base case scenario is when this photocatalyst was tested under low pressure CO_2 and using benzyl alcohol as a reactant which resulted in a CO production rate equal to 0.12μmol $g^{-1}h^{-1}$ after 22 h of reaction under illumination. When increasing the pressure to 60 bar, the CO production rate was increased by 125 times to 15μmol $g^{-1}h^{-1}$ (Fig. 6b). This significant enhancement in CO production rate can be explained by the increased CO_2 concentration in the liquid due to the high CO_2 pressure. A key aspect in the reaction is the CO_2 concentration in the liquid phase given that the reaction mainly happens in the phase where the photocatalyst is dispersed. This higher concentration is expected to have a positive impact by reducing the mass transfer limitation compared with the low-pressure reaction. The CO production rate was further increased by more than 280 times compared with the low-pressure reaction when employing supercritical CO_2. We explain this remarkable increase in CO production by the high pressure and temperature which further reduces the mass transfer limitation by maintaining a high CO_2 concentration in the liquid phase. When comparing this result with literature that used Cu_2O-based material as a photocatalyst for CO_2 reduction, the production rate is the highest reported and presented an ~ 600 % increase compared to other Cu_2O nanocube photocatalysts [20].

4. Conclusion

Cu_2O nanoparticles containing different amounts of Cu^0 were synthesized to be used as photocatalysts. These photocatalysts were characterized to investigate their composition, crystalline structure, morphology and photocatalytic activity. The photocatalyst containing small amounts of Cu^0 presented higher photocatalytic activity. The Cu_2O/Cu^0 photocatalyst was tested in the simultaneous photocatalytic activation of benzyl alcohol and CO_2. Simultaneous CO_2 reduction and benzyl alcohol activation was achieved under high-pressure and supercritical CO_2 conditions. The use of only high-pressure increased the production rate of CO by 125 times when compared to low pressure process. When increasing the pressure and the temperature to achieve supercritical CO_2, the production rate was remarkably increased by around 280 times when compared to the low-pressure process. This notable improvement in the CO production rate was almost 7 times higher than the highest reported in the literature for Cu_2O based photocatalysts. When analyzing the product of benzyl alcohol oxidation, hydrobenzoin was obtained as the main product which, to our knowledge, was not reported before for this photocatalyst. The production rate of hydrobenzoin was improved when using high-pressure and supercritical CO_2. When implementing high-pressure CO_2, the selectivity towards hydrobenzoin (C-C coupling product of two benzyl alcohol molecules) was increased to 98 %. To investigate the mechanism of the hydrobenzoin and CO production, thorough characterization in the remaining photocatalyst and control experiments were performed. A mechanism for the reaction was proposed, but in-situ analysis is needed to fully confirm the reaction mechanism and the formation of radicals under the reaction conditions. This opens a path for future research to thoroughly investigate the reaction mechanism under high-pressure conditions. When characterizing the Cu_2O/Cu^0 photocatalyst after reaction, CuO layer was detected as product of copper oxidation during the reaction. This change in the copper oxidation state suggests an avenue for further research, where a support material or a cocatalyst can be employed to mitigate this effect. The use of different alcohols in place of benzyl alcohol also paves the way for new research into the production of other high-value compounds. The process presented here can be applied to different photocatalysts in order to further improve the production rate of CO. This process in which high pressure CO_2 is used, has great potential to enhance the efficiency of CO_2 photocatalytic reduction while producing high value products.

CRediT authorship contribution statement

George Ebri: Writing – original draft, Visualization, Project administration, Methodology, Investigation, Formal analysis, Data curation, Conceptualization. **Essa Alhashmi:** Investigation. **Yasmine Baghdadi:** Investigation. **Matyas Daboczi:** Writing – review & editing, Investigation. **Salvador Eslava:** Writing – review & editing, Resources. **Klaus Hellgardt:** Writing – review & editing, Validation, Supervision, Project administration, Methodology, Funding acquisition, Conceptualization.

Declaration of competing interest

The authors declare that they have no known competing financial interests or personal relationships that could have appeared to influence the work reported in this paper.

Acknowledgements

G.E. and Y.B. would like to thank the Chemical Engineering Department of Imperial College London for financing their Ph.D. G.E. would like to thank Roberto Rocca Foundation for the fellowship to sponsor his PhD. M.D. and S.E. acknowledge the funding of the UK Engineering and Physical Sciences Research Council (EPSRC) provided via grant EP/S030727/1. The authors also thank the Analytical Service

of the Department of Chemical Engineering and the Department of Materials at Imperial College London for their help in performing the characterization presented in this work.

Appendix A. Supplementary data

Supplementary data to this article can be found online at https://doi.org/10.1016/j.cej.2024.158356.

Data availability

Data will be made available on request.

References

[1] Y. Zhou, Z. Wang, L. Huang, S. Zaman, K. Lei, T. Yue, Z.a. Li, B. You, B.Y. Xia, Engineering 2D photocatalysts toward carbon dioxide reduction, Adv. Energy Mater. 11 (8) (2021) 2003159.

[2] Z. Li, G. Zhu, W. Zhang, L. Zhu, B. Cao, J. Gao, X. Shi, Y. Huang, P. Liu, M. Hojamberdiev, Dual-functional copper (Cu0/Cu2+)-modified SrTiO3-δ nanosheets with enhanced photothermal catalytic performance for CO2 reduction and H2 evolution, Chem. Eng. J. 452 (2023) 139378, https://doi.org/10.1016/j.cej.2022.139378.

[3] N. Liu, N. Lu, K. Zhao, P. Liu, Z. Sun, J. Lu, Photocatalytic conversion of CH4 and CO2 to acetic acid over Cu/ZnO catalysts under mild conditions, Chem. Eng. J. 487 (2024) 150690, https://doi.org/10.1016/j.cej.2024.150690.

[4] K. Das, R. Das, M. Riyaz, A. Parui, D. Bagchi, A.K. Singh, A.K. Singh, C.P. Vinod, S. C. Peter, Intrinsic charge polarization in Bi19S27Cl3 nanorods promotes selective C□C coupling reaction during photoreduction of CO_2 to ethanol, Adv. Mater. 35 (5) (2023) 2205994.

[5] H. She, R. Hua, J. Zhao, Y. Xia, L. Wang, J. Huang, Q. Wang, Synergetic regulation of interfacial electronic structure of Cu, N co-doped carbon modified TiO_2 for efficient photocatalytic CO_2 reduction, Chem. Eng. J. 496 (2024) 153799, https://doi.org/10.1016/j.cej.2024.153799.

[6] C. Du, X. Wang, W. Chen, S. Feng, J. Wen, Y.A. Wu, CO_2 transformation to multicarbon products by photocatalysis and electrocatalysis, Mater. Today Adv. 6 (2020) 100071, https://doi.org/10.1016/j.mtadv.2020.100071.

[7] J. Fu, K. Jiang, X. Qiu, J. Yu, M. Liu, Product selectivity of photocatalytic CO_2 reduction reactions, Mater. Today 32 (2020) 222–243.

[8] L. Xu, Y. Ren, Y. Fu, M. Liu, F. Zhu, M. Cheng, J. Zhou, W. Chen, K. Wang, N. Wang, N. Li, Strong photo-thermal coupling effect boosts CO2 reduction into CH4 in a concentrated solar reactor, Chem. Eng. J. 468 (2023) 143831, https://doi.org/10.1016/j.cej.2023.143831.

[9] A.A. Khan, M. Tahir, Recent advancements in engineering approach towards design of photo-reactors for selective photocatalytic CO2 reduction to renewable fuels, J. CO2 Util. 29 (2019) 205–239.

[10] Y. Dong, P. Duchesne, A. Mohan, K.K. Ghuman, P. Kant, L. Hurtado, U. Ulmer, J. Y. Loh, A.A. Tountas, L. Wang, Shining light on CO_2: from materials discovery to photocatalyst, photoreactor and process engineering, Chem. Soc. Rev. 49 (16) (2020) 5648–5663.

[11] A. Raza, A.A. Haidry, Z. Yao, M.F. Saleem, A.A. Alothman, S. Mohammad, Synergistic effect of CuO and Sr doped g-C3N4 for CO_2 photoreduction into hydrocarbon fuels, Chem. Eng. J. 480 (2024) 148162, https://doi.org/10.1016/j.cej.2023.148162.

[12] L. Yuan, M.Y. Qi, Z.R. Tang, Y.J. Xu, Coupling strategy for CO_2 valorization integrated with organic synthesis by heterogeneous photocatalysis, Angew. Chem. 133 (39) (2021) 21320–21342.

[13] S. Kaneco, H. Kurimoto, K. Ohta, T. Mizuno, A. Saji, Photocatalytic reduction of CO_2 using TiO_2 powders in liquid CO_2 medium, J. Photochem. Photobiol. A Chem. 109 (1) (1997) 59–63.

[14] S. Kaneco, H. Kurimoto, Y. Shimizu, K. Ohta, T. Mizuno, Photocatalytic reduction of CO_2 using TiO_2 powders in supercritical fluid CO_2, Energy 24 (1) (1999) 21–30, https://doi.org/10.1016/S0360-5442(98)00070-X.

[15] N. Kometani, S. Hirata, M. Chikada, Photocatalytic reduction of CO_2 by Pt-loaded TiO_2 in the mixture of sub-and supercritical water and CO_2, J. Supercrit. Fluids 120 (2017) 443–447.

[16] S. Al Jitan, Y. Li, D. Bahamon, G. Žerjav, V.S. Tatiparthi, C. Aubry, M. Sinnokrot, Z. Matouk, N. Rajput, M. Gutierrez, K. Al-Ali, R. Hashaikeh, A. Pintar, L.F. Vega, G. Palmisano, Unprecedented photocatalytic conversion of gaseous and liquid CO_2 on graphene-impregnated Pt/Cu-TiO_2: the critical role of Cu dopant, J. Environ. Chem. Eng. 11 (2) (2023) 109485, https://doi.org/10.1016/j.jece.2023.109485.

[17] H. Liu, H.-L. Jiang, Solar-powered artificial photosynthesis coupled with organic synthesis, Chem 5 (10) (2019) 2508–2510, https://doi.org/10.1016/j.chempr.2019.09.006.

[18] S. Rej, M. Bisetto, A. Naldoni, P. Fornasiero, Well-defined Cu_2O photocatalysts for solar fuels and chemicals, J. Mater. Chem. A 9 (10) (2021) 5915–5951, https://doi.org/10.1039/D0TA10181H.

[19] M.E. Aguirre, R. Zhou, A.J. Eugene, M.I. Guzman, M.A. Grela, Cu_2O/TiO_2 heterostructures for CO_2 reduction through a direct Z-scheme: protecting Cu_2O from photocorrosion, Appl. Catal. B 217 (2017) 485–493.

[20] R. Lin, H. Chen, T. Cui, Z. Zhang, Q. Zhou, L. Nan, W.-C. Cheong, L. Schröck, V. Ramm, Q. Ding, X. Liang, S. Saris, F.J. Wendisch, S.A. Maier, R.A. Fischer, Y. Zhu, D. Wang, E. Cortes, Optimization of p-Type Cu_2O nanocube photocatalysts based on electronic effects, ACS Catal. 13 (17) (2023) 11352–11361, https://doi.org/10.1021/acscatal.3c02710.

[21] Y. Chen, M. Wang, Y. Ma, Y. Li, J. Cai, Z. Li, Coupling photocatalytic CO 2 reduction with benzyl alcohol oxidation to produce benzyl acetate over Cu 2 O/Cu, Cat. Sci. Technol. 8 (8) (2018) 2218–2223.

[22] Y. Zheng, L. Zhang, J. Guan, S. Qian, Z. Zhang, C.K. Ngaw, S. Wan, S. Wang, J. Lin, Y. Wang, Controlled synthesis of Cu0/Cu_2O for efficient photothermal catalytic conversion of CO_2 and H_2O, ACS Sustain. Chem. Eng. 9 (4) (2021) 1754–1761, https://doi.org/10.1021/acssuschemeng.0c07702.

[23] G. Ebri, K. Hellgardt, Flow synthesis development and photocatalytic activity optimization of copper oxide nanoparticles using design of experiments, Chem. Eng. J. 486 (2024) 150131, https://doi.org/10.1016/j.cej.2024.150131.

[24] X. Xiao, J. Jiang, L. Zhang, Selective oxidation of benzyl alcohol into benzaldehyde over semiconductors under visible light: The case of Bi12O17Cl2 nanobelts, Appl. Catal. B 142–143 (2013) 487–493, https://doi.org/10.1016/j.apcatb.2013.05.047.

[25] X. Sun, D. Jiang, L. Zhang, W. Wang, Alkaline modified g-C3N4 photocatalyst for high selective oxide coupling of benzyl alcohol to benzoin, Appl. Catal. B 220 (2018) 553–560.

[26] H. Wen, W. Duan, L. Guo, Q. Wang, X. Fu, Y. Wang, R. Li, B. Jin, R. Du, C. Yang, Directing charge transfer in a chemical-bonded Ni/Cd0. 7Mn0. 3S Schottky heterojunction for selective photocatalytic oxidation of benzyl alcohol structural organic platform molecules coupled with hydrogen evolution reaction, Appl. Catal. b: Environ. Energy 345 (2024) 123641.

[27] L. Wei, R. Song, J. Song, Y. Li, Y. Nie, L. Liu, J. Wan, Thiophene-containing conjugated polymers modified Zn0.5Cd0.5S inorganic/organic S-scheme heterojunction for boosting photocatalytic hydrogen production coupled with benzyl alcohol oxidation, Chem. Eng. J. 496 (2024) 154107, https://doi.org/10.1016/j.cej.2024.154107.

[28] L. Wang, Z. Huang, S. Xie, Q. Zhang, H. Wang, Y. Wang, Photocatalytic C− H activation and C− C coupling of monohydric alcohols, Catal. Commun. 153 (2021) 106300.

[29] S.G. Lee, M.J. Kang, M. Park, K.-J. Kim, H. Lee, H.S. Kim, Selective photocatalytic conversion of benzyl alcohol to benzaldehyde or deoxybenzoin over ion-exchanged CdS, Appl. Catal. B 304 (2022) 120967, https://doi.org/10.1016/j.apcatb.2021.120967.

[30] S. Mandal, S.P. Nanavati, D.J. Willock, R. Ananthakrishnan, Band gap engineering of amine functionalized Ag(I)-based coordination polymers and their plasmonic Ag0 coupled novel visible light driven photo-redox system for selective oxidation of benzyl alcohol, Appl. Catal. B 303 (2022) 120821, https://doi.org/10.1016/j.apcatb.2021.120821.

[31] G. Han, X. Liu, Z. Cao, Y. Sun, Photocatalytic pinacol C–C coupling and jet fuel precursor production on $ZnIn_2S4$ nanosheets, ACS Catal. 10 (16) (2020) 9346–9355, https://doi.org/10.1021/acscatal.0c01715.

[32] Z. Huang, P. Sun, H. Zhang, H. Zhang, S. Zhang, Z. Chen, X. Yi, S. Xie, Solar-driven highly effective biomass-derived alcohols C–C coupling integrated with H_2 production by CdS quantum dots modified Zn2In2S5 nanosheets, ACS Catal. 14 (7) (2024) 4581–4592.

[33] X. Wu, X. Fan, S. Xie, I. Scodeller, X. Wen, D. Vangestel, J. Cheng, B. Sels, Zinc-indium-sulfide favors efficient C − H bond activation by concerted proton-coupled electron transfer, Nat. Commun. 15 (1) (2024) 4967, https://doi.org/10.1038/s41467-024-49265-2.

[34] Z. Chen, M.Z. Shahid, X. Jiang, M. Zhang, D. Pan, H. Xu, G. Jiang, J. Wang, Z. Li, Regulating the active sites of Cs2AgBiCl6 by doping for efficient coupling of photocatalytic CO_2 reduction and benzyl alcohol oxidation, Small 20 (1) (2024) 2304756.

[35] Y. Wang, J. Pu, J. An, X. Liang, W. Li, Y. Huang, J. Yang, T. Chen, Y. Yao, Tailoring charge separation in ZnIn2S4@ CdS hollow nanocages for simultaneous alcohol oxidation and CO_2 reduction under visible light, Inorg. Chem. (2024).

[36] M. Staniuk, D. Zindel, W. van Beek, O. Hirsch, N. Kränzlin, M. Niederberger, D. Koziej, Matching the organic and inorganic counterparts during nucleation and growth of copper-based nanoparticles – in situ spectroscopic studies, CrstEngComm 17 (36) (2015) 6962–6971, https://doi.org/10.1039/C5CE00454C.

[37] Y. Baghdadi, F. Temerov, J. Cui, M. Daboczi, E. Rattner, M.S. Sena, I. Itskou, S. Eslava, Cs3Bi2Br9/g-C3N4 direct Z-scheme heterojunction for enhanced photocatalytic reduction of CO_2 to CO, Chem. Mater. 35 (20) (2023) 8607–8620, https://doi.org/10.1021/acs.chemmater.3c01635.

[38] Y.A. Wu, I. McNulty, C. Liu, K.C. Lau, Q. Liu, A.P. Paulikas, C.-J. Sun, Z. Cai, J. R. Guest, Y. Ren, Facet-dependent active sites of a single Cu2O particle photocatalyst for CO_2 reduction to methanol, Nat. Energy 4 (11) (2019) 957–968.

[39] A. Paracchino, V. Laporte, K. Sivula, M. Grätzel, E. Thimsen, Highly active oxide photocathode for photoelectrochemical water reduction, Nat. Mater. 10 (6) (2011) 456–461, https://doi.org/10.1038/nmat3017.

[40] M.C. Biesinger, L.W.M. Lau, A.R. Gerson, R.S.C. Smart, Resolving surface chemical states in XPS analysis of first row transition metals, oxides and hydroxides: Sc, Ti, v, Cu and Zn, Appl. Surf. Sci. 257 (3) (2010) 887–898, https://doi.org/10.1016/j.apsusc.2010.07.086.

[41] Y. Xin, K. Yu, L. Zhang, Y. Yang, H. Yuan, H. Li, L. Wang, J. Zeng, Copper-based plasmonic catalysis: recent advances and future perspectives, Adv. Mater. 33 (32) (2021) 2008145, https://doi.org/10.1002/adma.202008145.

[42] J.A. Creighton, D.G. Eadon, Ultraviolet–visible absorption spectra of the colloidal metallic elements, J. Chem. Soc. Faraday Trans. 87 (24) (1991) 3881–3891.

[43] M. Daboczi, J. Cui, F. Temerov, S. Eslava, Scalable all-inorganic halide perovskite photoanodes with >100 h operational stability containing earth-abundant materials, Adv. Mater. 35 (45) (2023) 2304350, https://doi.org/10.1002/adma.202304350.

[44] Y. Baghdadi, M. Daboczi, F. Temerov, M. Yang, J. Cui, S. Eslava, A g-C3N4/rGO/Cs3Bi2Br9 mediated Z-scheme heterojunction for enhanced photocatalytic CO_2 reduction, J. Mater. Chem. A 12 (27) (2024) 16383–16395, https://doi.org/10.1039/D4TA01857E.
[45] B. Ma, C. Kong, J. Lv, W. Zhang, J. Guo, X. Zhang, Z. Yang, S. Yang, Controllable in-situ synthesis of Cu–Cu_2O heterostructures with enhanced visible-light photocatalytic activity, ChemistrySelect 3 (38) (2018) 10641–10645.
[46] R. Beranek, (Photo) electrochemical methods for the determination of the band edge positions of TiO2-based nanomaterials, Adv. Phys. Chem. 2011 (2011).
[47] M.-Y. Qi, Q. Lin, Z.-R. Tang, Y.-J. Xu, Photoredox coupling of benzyl alcohol oxidation with CO_2 reduction over CdS/TiO2 heterostructure under visible light irradiation, Appl. Catal. b: Environ. Energy 307 (2022) 121158.
[48] M.Y. Qi, Y.J. Xu, Efficient and direct functionalization of allylic sp3 C− H bonds with concomitant CO_2 reduction, Angew. Chem. 135 (2023) e202311731.
[49] F.-K. Shang, Y.-H. Li, M.-Y. Qi, Z.-R. Tang, Y.-J. Xu, Photocatalytic materials for sustainable chemistry via cooperative photoredox catalysis, Catal. Today 410 (2023) 85–101.
[50] S. Yu, Y. Jiang, Y. Sun, F. Gao, W. Zou, H. Liao, L. Dong, Real time imaging of photocatalytic active site formation during H2 evolution by in-situ TEM, Appl Catal B 284 (2021) 119743.
[51] S. Xie, Z. Shen, J. Deng, P. Guo, Q. Zhang, H. Zhang, C. Ma, Z. Jiang, J. Cheng, D. Deng, Y. Wang, Visible light-driven C−H activation and C–C coupling of methanol into ethylene glycol, Nat. Commun. 9 (1) (2018) 1181, https://doi.org/10.1038/s41467-018-03543-y.
[52] S. Kreft, R. Schoch, J. Schneidewind, J. Rabeah, E.V. Kondratenko, V. A. Kondratenko, H. Junge, M. Bauer, S. Wohlrab, M. Beller, Improving selectivity and activity of CO_2 reduction photocatalysts with oxygen, Chem 5 (7) (2019) 1818–1833, https://doi.org/10.1016/j.chempr.2019.04.006.
[53] K. Nakaoka, J. Ueyama, K. Ogura, Photoelectrochemical behavior of electrodeposited CuO and Cu2 O thin films on conducting substrates, J. Electrochem. Soc. 151 (10) (2004) C661.
[54] D. Jiang, J. Xue, L. Wu, W. Zhou, Y. Zhang, X. Li, Photocatalytic performance enhancement of CuO/Cu2O heterostructures for photodegradation of organic dyes: effects of CuO morphology, Appl Catal B 211 (2017) 199–204.
[55] D. Jeong, W. Jo, J. Jeong, T. Kim, S. Han, M.-K. Son, H. Jung, Characterization of Cu 2 O/CuO heterostructure photocathode by tailoring CuO thickness for photoelectrochemical water splitting, RSC Adv. 12 (5) (2022) 2632–2640.
[56] X. Zhang, X. Zhao, K. Chen, Y. Fan, S. Wei, W. Zhang, D. Han, L. Niu, Palladium-modified cuprous (i) oxide with 100 facets for photocatalytic CO_2 reduction, Nanoscale 13 (5) (2021) 2883–2890.
[57] X. Zhao, L. Sun, X. Jin, M. Xu, S. Yin, J. Li, X. Li, D. Shen, Y. Yan, P. Huo, Cu media constructed Z-scheme heterojunction of UiO-66-NH2/Cu2O/Cu for enhanced photocatalytic induction of CO_2, Appl. Surf. Sci. 545 (2021) 148967.